

# Muonium as a hydrogen analogue in silicon and germanium; quantum effects and hyperfine parameters

A. R. Porter, M. D. Towler and R. J. Needs  
*TCM Group, Cavendish Laboratory,  
 Madingley Road, Cambridge, CB3 0HE, UK*  
 (May 8, 2018)

We report a first-principles theoretical study of hyperfine interactions, zero-point effects and defect energetics of muonium and hydrogen impurities in silicon and germanium. The spin-polarized density functional method is used, with the crystalline orbitals expanded in all-electron Gaussian basis sets. The behaviour of hydrogen and muonium impurities at both the tetrahedral and bond-centred sites is investigated within a supercell approximation. To describe the zero-point motion of the impurities, a double adiabatic approximation is employed in which the electron, muon/proton and host lattice degrees of freedom are decoupled. Within this approximation the relaxation of the atoms of the host lattice may differ for the muon and proton, although in practice the difference is found to be slight. With the inclusion of zero-point motion the tetrahedral site is energetically preferred over the bond-centred site in both silicon and germanium. The hyperfine and superhyperfine parameters, calculated as averages over the motion of the muon, agree reasonably well with the available data from muon spin resonance experiments.

## I. INTRODUCTION

Hydrogen is known to have a wide range of physical effects in semiconductors, including the passivation of states associated with deep-level impurities, enhancement of the diffusivity of oxygen, and the formation of large, planar structures known as platelets. [1] It is present in large quantities during the processing stages of device manufacture and is one of the commonest impurities in technologically important materials such as silicon and germanium. Since such hydrogen impurities can have significant effects on semiconductor electrical properties, a more complete understanding of their behaviour at the microscopic level is desirable.

Paramagnetic hydrogen centres can in principle be studied using the electron paramagnetic resonance (EPR) technique. Information on their local environment is obtained by following the time evolution of the signal corresponding to the coupling of the spin of the impurity with an external electromagnetic field. However, few studies have been reported for hydrogen in semiconductors because the hydrogen atoms are mobile and diffuse to defects where they form passivated complexes. The transient centres of isolated hydrogen impurities are nevertheless of significant interest because of their involvement in diffusion processes, and in fact they may be studied using muon spin resonance ( $\mu$ SR) techniques. Muons have the same charge as protons but only about one ninth of the mass. They can capture an electron to form a hydrogen-like bound state known as muonium (given the symbol Mu), and it is thus possible to consider the muon as a proton analogue. Transient centres of implanted positive muons in semiconductors may be studied as the muon has a lifetime of just 2.2  $\mu$ s and diffuses to locally stable sites within a few nanoseconds. The short lifetime also

means that there is almost never more than one muon in the sample at any one time, and that the distribution of muons does not reach true thermal equilibrium. In a muon spin resonance experiment fully polarized positive muons are injected into the sample, and by observing the positrons produced by the decay of the muons one can obtain information about the defect. [1]

When  $\mu$ SR experiments are performed on silicon or germanium, two different hyperfine signals are observed. One of these is entirely isotropic while the other has an anisotropic (dipolar) component with uniaxial symmetry along the [1 1 1] axis. [1] The impurity responsible for the former signal is usually referred to as normal muonium (Mu) and that for the latter, anomalous muonium (Mu\*). Normal muonium has been identified as muonium in the interstitial region, probably in the vicinity of the tetrahedral (T) interstitial site. Symons and Cox [2] first suggested that anomalous muonium corresponds to a neutral muonium at the bond-centred (BC) site and this has been borne out by a number of theoretical studies. The various experimental data for muonium in silicon have been interpreted in terms of a configuration-coordinate diagram. [3]

The majority of recent theoretical work in this area has been at the first principles level within an adiabatic approximation, using the local spin density (LSDA) or generalized gradient (GGA) approximations to density functional theory (DFT). [4] Calculations using pseudopotentials and plane-wave basis sets [5–7] have been reasonably successful in reproducing the hyperfine and superhyperfine parameters observed in experiments. The majority of such calculations appear to demonstrate that hydrogen impurities at the T and BC sites have similar energies. [7,8]

The application of the Feynman path-integral [9]

method to the study of these systems enables the effect of the quantum nature of the muon to be studied directly at finite temperatures. However, the large computational demands of such an approach have limited its use to date. Ramírez and Herrero [10] used the path integral molecular dynamics method to study hydrogen and muonium in silicon with the H/Mu-Si interaction described by an empirical three-body potential. However, the results appear to be in conflict with experiment. Recently, Miyake *et al.* [11] applied the path-integral Monte Carlo technique to the study of hydrogen and muonium at the T site in silicon, with the electron-electron interactions described within the LDA. Despite finding the T site to be a local maximum on the potential energy surface, they found the muon distribution to be peaked at that site because of the quantum motion.

In this work we employ all-electron DFT calculations within a double adiabatic approximation to study muonium and hydrogen at the BC and T sites in silicon and germanium. The use of all-electron calculations allows an assessment of the accuracy of the correction procedures which are used to obtain the hyperfine and superhyperfine parameters in pseudopotential calculations. [6] The use of a double adiabatic approximation allows us to obtain both the zero-point energy and wave function of the impurity. Our inclusion of the zero-point motion is at a level beyond that in previous first principles calculations since the positions of the host silicon or germanium atoms are allowed to relax in the presence of the zero-point motion of the impurity. At this level of approximation the relaxations of the host lattice are different for a muon and a proton. Our calculations thus allow an assessment of the differences in the potentials felt by the two impurities, thereby testing one of the assumptions underlying the configuration-coordinate diagram [3] used to interpret experimental data.

## II. METHOD

### A. All-electron spin-polarized LSDA-DFT calculations

All the first principles calculations reported here were performed with the CRYSTAL95 software package [12]. The (zero temperature) spin-polarized density functional method [13,14] was used, together with both local density and gradient corrected approximations to the exchange-correlation functional (namely the Perdew-Zunger LSDA [15] and the PW91 form of the GGA [16]). The calculations were performed within a periodic supercell approach with a single hydrogen impurity in supercells containing either sixteen or fifty-four silicon or germanium atoms. Fig. 1 shows the relaxed atomic environments of a single muon at both bond-centred and tetrahedral impurity sites in silicon. The measured lat-

tice constants (5.429 Å for silicon and 5.6579 Å for germanium) were used in all calculations.

Other approximations made were as follows. The use of local basis functions requires the real space Coulomb and exchange series to be limited and approximated as described in references [12,17]; the accuracy with which the various Gaussian integrals are computed is controlled by classifying basis function pairs according to overlap or penetration criteria defined by five parameters, which in this study were set to  $10^{-7}$ ,  $10^{-6}$ ,  $10^{-7}$ ,  $10^{-7}$  and  $10^{-14}$ . [12] This is normally sufficient to give a numerical error of less than 0.001 eV/atom in the relative energies of different structures. The reciprocal space integrations necessary to reconstruct the density matrix in real space at each self-consistent cycle were approximated by summing over a set of k-points belonging to a mesh of Monkhorst-Pack [18] type which was centred on the origin in reciprocal space. The convergence of both the total energy and the isotropic hyperfine parameter of the muon with respect to the reciprocal space sampling density was investigated. A  $4 \times 4 \times 4$  k-point mesh was found to be sufficient for the 16-atom supercell. With this mesh, the total energy and isotropic hyperfine parameter are within 0.0025 eV/atom and 3 MHz of their fully converged values, respectively. A  $3 \times 3 \times 3$  k-point mesh was used for the 54-atom supercell, which also gives excellent convergence. The convergence of various quantities with respect to the supercell size and basis set is discussed in Section III.

A hydrogen impurity introduces a defect state into the band gap of the host crystal. Finite supercell sizes give rise to interactions between the defects in different cells and thus to a small but potentially significant dispersion in the defect band. This dispersion could lead, for example, to overlap of the majority spin defect band with the minority spin defect band and/or the silicon valence/conduction bands. In either case an unphysical conducting state is formed. This problem is not entirely eliminated even with the use of the larger 54-atom supercell. However, judicious use of the level-shifting convergence technique [12,19] allows a small decoupling of unoccupied and occupied states which prevents the system entering a conducting state. Population analysis of the final self-consistent wave function revealed that each supercell contained a single extra majority spin electron as expected on physical grounds. The calculations thus correctly model this aspect of the behaviour of a single impurity in a large crystal, which is necessary in order to obtain physical hyperfine and superhyperfine parameters.

### B. Gaussian Basis Sets

The Bloch functions required to expand the Kohn-Sham orbitals in the solid-state band structure problem are built from periodic arrays of atom-centred Gaussian functions. One motivation for the use of such a basis set

is that all electrons in the system may be treated explicitly, allowing the spin density at and around the nucleus (and hence the hyperfine parameters) to be calculated directly without resorting to correction procedures of the sort required in pseudopotential calculations. [6]

The basis set used for the majority of the silicon calculations was of the type  $s(8)sp(8)sp(3)sp(1)$  where the numbers in brackets refer to the number of contracted primitive Gaussians making up each shell. For convergence checking we also used a higher quality silicon set with an additional  $d$  polarization function of the type  $s(8)sp(8)sp(1)sp(1)sp(1)d(1)$ . The basis set used for the germanium calculations was  $s(9)sp(7)sp(6)sp(3)sp(1)d(6)d(1)$ .

To describe the hydrogen atom, an uncontracted basis of eleven  $s$  functions and a single  $p$  function was used. Such a large set (mainly consisting of functions with relatively high exponents) was found to be necessary to compute accurate hyperfine parameters. A spin-unrestricted Hartree-Fock calculation of the total energy of the free atom with this basis gave  $-0.49988$  Ha which is close to the exact result of  $-0.5$  Ha. The isotropic hyperfine parameter was  $1421.9$  MHz compared with that obtained from the exact wave function of  $1422.8$  MHz. The corresponding values obtained from an LSDA-DFT calculation with this basis set were  $-0.47833$  Ha (which is very close to the value of  $-0.47885$  Ha obtained from an atomic code using integration on a very fine grid) and  $1356.6$  MHz.

Optimal Gaussian basis sets for use in close packed solids are significantly different from those appropriate to the atomic and molecular cases. In particular, careful optimization is required to avoid the problems of linear dependence and basis set superposition error due to the overlap of diffuse functions. In this study we used the following procedure. All basis set parameters were first optimized in the free atom. The exponents and contraction coefficients of the valence functions in silicon and germanium were then reoptimized in the pure bulk material. Finally, a hydrogen atom was inserted at a bond-centred site, the positions of the nearest-neighbour silicon/germanium atoms relaxed, and the parameters of the valence functions of each atom again reoptimized. To test the transferability of the optimized basis sets the hydrogen was displaced from the BC site along the bond by  $0.27$  Å, and the basis function parameters were reoptimized for the new geometry. The energy as a function of displacement along the bond was calculated for each of these two basis sets. The variation in energy was essentially the same.

The final exponents and contraction coefficients of all the basis sets employed in this study are available elsewhere. [20]

It is important to investigate the possibility of basis set superposition error (BSSE) in defect energetics calculations for a system described by a localized basis. The basis sets for the host lattice atoms are necessarily incomplete. Insertion of an impurity atom allows additional

variational freedom in the description of the atoms adjacent to the defect site, particularly when the impurity is described by a relatively diffuse basis set. This can distort the relative stabilities of defects at impurity sites of differing local coordination number and geometry. In the present case, the hydrogen impurity is considerably closer to its neighbours at the BC site than at the T site, and thus one might expect the BC site to be artificially stabilized with respect to the T.

This expectation is confirmed by an estimate of the BSSE using a counterpoise correction. [21] For the 16-atom supercell, addition of “ghost” hydrogen basis functions into the relaxed silicon lattice lowered the energy per cell by  $0.199$  eV (BC site) and  $0.068$  eV (T site) with the smaller silicon basis, and by  $0.0533$  eV (BC site) and  $0.0243$  eV (T site) with the larger silicon basis. In germanium, the energy is lowered by  $0.251$  eV (BC site) and  $0.0534$  eV (T site) by the same procedure. Inclusion of a lattice of “ghost” silicon/germanium functions around a hydrogen atom lowered the energy by less than  $0.0005$  eV. These numbers may be taken to give a rough indication of basis set incompleteness in each case. It can thus be concluded that in silicon the BSSE lowers the energy of the BC site over that of the T site by around  $0.13$  eV with the smaller basis, but by only  $0.03$  eV with the larger set. The corresponding correction for the germanium case is  $0.20$  eV.

### C. Calculation of zero-point motion

For the calculation of the zero-point motion of the muon/proton a double adiabatic approximation was used. This means that the motions of the electrons and of the muon are considered to be decoupled from the motion of the atomic nuclei, and furthermore that the electronic motion is decoupled from that of the muon. The approximation is justified by the fact that a muon is roughly 207 times more massive than an electron and around 243 times less massive than a silicon nucleus. For a proton the equivalent factors are respectively 1836 and 28; the decoupling of the proton and silicon motion is thus somewhat less justified. The mass differences are of course more favourable for the heavier germanium nucleus.

The positions of the silicon/germanium nuclei are denoted by  $\mathbf{r}_n$ , the muon or proton positions by  $\mathbf{r}_\mu$ , and the electron positions by  $\mathbf{r}_e$ . The double adiabatic approximation is used to decouple the motions of the particles by approximating the wave function as a product of nuclear, muon/proton and electronic parts,

$$\Psi(\mathbf{r}_e, \mathbf{r}_\mu, \mathbf{r}_n) = \psi^n(\mathbf{r}_n) X^\mu(\mathbf{r}_\mu; \mathbf{r}_n) \phi^e(\mathbf{r}_e; \mathbf{r}_\mu, \mathbf{r}_n), \quad (2.1)$$

where the variables to the right of the semi-colons appear as parameters and those to the left are dynamical variables. Within the double adiabatic approximation the

three wave functions each satisfy separate Schrödinger equations:

$$\hat{H}_e(\mathbf{r}_e; \mathbf{r}_\mu, \mathbf{r}_n) \phi^e(\mathbf{r}_e; \mathbf{r}_\mu, \mathbf{r}_n) = E^e(\mathbf{r}_\mu, \mathbf{r}_n) \phi^e(\mathbf{r}_e; \mathbf{r}_\mu, \mathbf{r}_n) , \quad (2.2)$$

$$\hat{H}_\mu(\mathbf{r}_\mu; \mathbf{r}_n) X_\alpha^\mu(\mathbf{r}_\mu; \mathbf{r}_n) = E_\alpha^\mu(\mathbf{r}_n) X_\alpha^\mu(\mathbf{r}_\mu; \mathbf{r}_n) , \quad (2.3)$$

$$\hat{H}_n \psi_\alpha^n(\mathbf{r}_n) = E_\alpha^n \psi_\alpha^n(\mathbf{r}_n) . \quad (2.4)$$

The subscript  $\alpha$  labels the different eigenstates of the muon. Although only the ground state of the nuclear wave function is considered here, it is also labelled by  $\alpha$  since it depends on the chosen muon eigenstate. The different electronic eigenstates are not labelled, since it is only the ground state of the electronic wave function as a function of the muon and nuclear positions that is of interest in the current work. The three Hamiltonians are:

$$\begin{aligned} \hat{H}_e(\mathbf{r}_e; \mathbf{r}_\mu, \mathbf{r}_n) &= \hat{T}_e(\mathbf{r}_e) + V_{ee}(\mathbf{r}_e) \\ &+ V_{en}(\mathbf{r}_e, \mathbf{r}_n) + V_{e\mu}(\mathbf{r}_e, \mathbf{r}_\mu) , \end{aligned} \quad (2.5)$$

$$\begin{aligned} \hat{H}_\mu(\mathbf{r}_\mu; \mathbf{r}_n) &= \hat{T}_\mu(\mathbf{r}_\mu) + V_{\mu\mu}(\mathbf{r}_\mu) + V_{\mu n}(\mathbf{r}_\mu, \mathbf{r}_n) \\ &+ E^e(\mathbf{r}_\mu, \mathbf{r}_n) , \end{aligned} \quad (2.6)$$

$$\hat{H}_n(\mathbf{r}_n) = V_{nn}(\mathbf{r}_n) + E_\alpha^\mu(\mathbf{r}_n) . \quad (2.7)$$

where  $\hat{T}$  is the kinetic operator and  $V_{ab}$  is the Ewald interaction between particles of types  $a$  and  $b$ . The term  $V_{\mu\mu}$  is a constant describing the interactions between the impurity atoms in the different supercells. The electronic energy,  $E^e$ , appears as an effective potential in the muonic Hamiltonian, Eq. 2.7. Hence, when Eq. 2.3 is solved, the resulting energy includes the electronic contribution. This energy then appears in the nuclear Hamiltonian as an effective potential. Thus the total energy of the system is given by the eigenvalue in Eq. 2.4.

In order to find a good starting point for the BC calculations we performed LSDA calculations with the muon/proton fixed at the bond centre. The positions of the nearest and next-nearest neighbour (NN and NNN) silicon/germanium atoms were then relaxed. For the T site the muon/proton was held fixed at the T site while the four NN silicon/germanium atoms were relaxed in the radial direction.

The next step is to calculate the potential experienced by the muon/proton in the crystal by solving the electronic Schrödinger equation (2.2) within the LSDA, as a function of the parameters  $\mathbf{r}_\mu$  and  $\mathbf{r}_n$ . For the BC site calculations, the parameters  $\mathbf{r}_n$  were varied by considering four different additional relaxations of the NN silicon atoms along the  $[1\ 1\ 1]$  direction. For each of the positions of the NN silicon atoms, the NNN atoms were relaxed.

We then performed a further twelve LSDA calculations as a function of the position of the muon/proton for each of these nuclear configurations in order to map out the required potential energy surfaces. A similar procedure was used for germanium. For the T site the static relaxation of the NN atoms is very small and we assumed that the zero-point motion of the muon/proton would not give any additional relaxation.

In order to solve Eq. 2.3 for the muon/proton wave function we used a fitted polynomial for the energy  $E^e(\mathbf{r}_\mu, \mathbf{r}_n)$ . For the BC site we use a cylindrical coordinate system with the origin at the BC site and the  $z$ - and  $\rho$ -coordinates directed along the bond and in the plane perpendicular to the bond, respectively. We have neglected the  $\theta$  dependence of the potential. This assumption was checked by displacing the muon by 0.53 Å from the BC site along the  $[-1\ 1\ 0]$  direction and then rotating it about the  $[1\ 1\ 1]$  axis. The maximum variation seen in the energy of the 16-atom supercell during the rotation was just 0.002 eV. The Taylor expansion of the cylindrically symmetric potential, neglecting sixth-order terms and higher, is

$$V_{BC}(\rho, z) = V_{BC}(0, 0) + \beta\rho^2 + \gamma z^2 + \delta\rho^2 z^2 + \zeta\rho^4 + \eta z^4 . \quad (2.8)$$

As a further simplification in order to avoid costly, low-symmetry calculations, the  $\delta\rho^2 z^2$  term was neglected. The resulting Schrödinger equation is separable. In order to check the assumption of  $\rho$ - $z$  separability, a few calculations were performed with the muon at points where both the  $\rho$  and  $z$  coordinates were non-zero. These energies were then compared with those predicted by the fitted potential neglecting the term in  $\rho^2 z^2$ . The errors due to neglecting the  $\rho^2 z^2$  term increased only slowly away from the BC site, and the corresponding error in the ground state energy is small because the wave function of the muon/proton is localized around the BC site.

Our approximation formula was then obtained by a least-squares fit of the twelve energies calculated at different values of  $\mathbf{r}_\mu$  (for fixed  $\mathbf{r}_n$ ) to the resulting polynomial. The fitted values of the parameters in Eq. 2.8 used in the calculations of the zero-point energies for silicon and germanium are given in Table I.

The polynomial expansion for the energy surface around the T site is the Taylor expansion which is invariant under all of the 24 rotations forming the group  $T_d$ . Cartesian coordinates centred at the T site were used, and in order to obtain a good fit to the energy surface it was found necessary to include terms up to sixth order:

$$\begin{aligned} V_T(x, y, z) &= V_T(0, 0, 0) + a_2(x^2 + y^2 + z^2) + a_3xyz \\ &+ a_4(x^4 + y^4 + z^4) + b_4(x^2 y^2 + x^2 z^2 + y^2 z^2) \\ &+ a_5 xyz(x^2 + y^2 + z^2) + a_6(x^6 + y^6 + z^6) \\ &+ b_6(x^2 y^4 + x^2 z^4 + x^4 y^2 + x^4 z^2 + y^2 z^4 \\ &+ y^4 z^2) + c_6 x^2 y^2 z^2 . \end{aligned} \quad (2.9)$$

The fitted values of the parameters in this equation are given in Table II.

The solution of the muon/proton Schrödinger equation (2.3) was performed by diagonalizing within a basis of harmonic oscillator eigenfunctions centred on either the BC or T site. We constructed muon and proton basis sets consisting of the solutions of the harmonic part of the calculated potentials:

$$V_{0\text{BC}} = V_{\text{BC}}(0, 0, 0) + \beta(x^2 + y^2) + \gamma z^2, \quad (2.10)$$

and

$$V_{0\text{T}} = V_{\text{T}}(0, 0, 0) + a_2(x^2 + y^2 + z^2). \quad (2.11)$$

For a harmonic potential, the Schrödinger equation may be solved by separation of variables:

$$X(\mathbf{r}_\mu) = \mathcal{X}(x)\mathcal{Y}(y)\mathcal{Z}(z).$$

This gives three separate equations for  $\mathcal{X}$ ,  $\mathcal{Y}$ , and  $\mathcal{Z}$ , whose solutions are of the form:

$$\mathcal{X}_l(x') = A_l H_l(x') e^{-\frac{1}{2}x'^2}, \quad (2.12)$$

where  $A_l = \frac{1}{\sqrt{2^l \pi^{\frac{1}{2}} l!}}$  is the normalisation factor,  $x' = (2MC_x)^{\frac{1}{4}} x$  is a rescaled variable which allows the eigenfunctions to be written in terms of the standard Hermite polynomials,  $H_l(x')$ , and  $C_x$  is the appropriate harmonic coefficient. The associated energy eigenvalues are

$$E_{\lambda_l} = \left(l + \frac{1}{2}\right) \left(\frac{2C_\lambda}{M}\right)^{\frac{1}{2}}, \quad (2.13)$$

where  $\lambda$  runs over the three directions,  $x$ ,  $y$ , and  $z$ , and  $C_\lambda$  is the harmonic coefficient corresponding to that direction. The value of the mass,  $M$ , of the particle depends on whether we are solving for the proton or muon wave function.

Having constructed our basis functions we now consider the full potentials which are written as the sum of harmonic and anharmonic terms:

$$V_{\text{BC}} = V_{0\text{BC}} + \Delta V_{\text{BC}} \quad (2.14)$$

$$V_{\text{T}} = V_{0\text{T}} + \Delta V_{\text{T}}. \quad (2.15)$$

The Hamiltonian matrix elements were calculated in the basis of the harmonic solutions and the resulting matrix equations were diagonalized. A basis set constructed from all Hermite polynomials up to and including eighth order and containing a total of 729 basis functions was found to be sufficient to obtain converged values for at least the lowest six eigenvalues,  $E_\alpha^\mu(\mathbf{r}_n)$ , of the system with the muon/proton at the BC site. At the T site it was found necessary to increase the size of the basis set to include all Hermite polynomials up to twelfth order, which gave 2197 functions.

The solution of Eq. 2.7 is trivial as the operator is multiplicative and the eigenfunctions are delta functions. The total energy,  $E_\alpha^n$ , is therefore the sum of  $E_\alpha^\mu(\mathbf{r}_n)$  and the Ewald energy of the lattice of host atoms,  $V_{nn}(\mathbf{r}_n)$ .

## D. Hyperfine and superhyperfine parameters and motion averaging

The components of the hyperfine tensor,  $\mathbf{A}$ , define the spin Hamiltonian for the hyperfine interaction between the spins of an electron and a nucleus:

$$\hat{\mathcal{H}}_s = \mathbf{S}_e \cdot \mathbf{A} \cdot \mathbf{S}_n. \quad (2.16)$$

The hyperfine tensor is normally split into isotropic and anisotropic parts,

$$\mathbf{A} = A_s \mathbf{I} + \mathbf{A}_p, \quad (2.17)$$

where  $\mathbf{I}$  is the  $(3 \times 3)$  unit matrix. The isotropic hyperfine parameter (or *superhyperfine* parameter when it is calculated at one of the nearest neighbours of the impurity) is given by

$$\begin{aligned} A_s &= \frac{2\mu_0}{3} g_e \mu^e g_n \mu^n \rho_\sigma(\mathbf{r}_n) \\ &= 104.982 \gamma^n \rho_\sigma(\mathbf{r}_n) \text{ [MHz]}. \end{aligned} \quad (2.18)$$

where  $\mu_0$  is the permeability of free space,  $\mu^e$  is the Bohr magneton,  $\mu^n$  is the nuclear magneton and  $g_e$  and  $g_n$  are the electron and nuclear  $g$  factors. [22] The position of the nucleus is denoted by  $\mathbf{r}_n$  and  $\rho_\sigma = \rho_\uparrow - \rho_\downarrow$  [bohr<sup>-3</sup>]. [23]

The anisotropic part of the hyperfine tensor is given by

$$\begin{aligned} \mathbf{A}_p &= \frac{\mu_0}{4\pi} g_e \mu^e g_n \mu^n \int \mathbf{T}(\mathbf{r}) \rho_\sigma(\mathbf{r} + \mathbf{r}_n) d\mathbf{r} \\ &= 12.531 \gamma^n \int \mathbf{T}(\mathbf{r}) \rho_\sigma(\mathbf{r} + \mathbf{r}_n) d\mathbf{r} \text{ [MHz]} \end{aligned} \quad (2.19)$$

where  $\mathbf{T}(\mathbf{r})$  is a traceless tensor,

$$\mathbf{T}(\mathbf{r}) = \frac{1}{r^5} \begin{pmatrix} 3x^2 - r^2 & 3xy & 3xz \\ 3xy & 3y^2 - r^2 & 3yz \\ 3xz & 3yz & 3z^2 - r^2 \end{pmatrix}, \quad (2.20)$$

and the origin of coordinates is on the nucleus at  $\mathbf{r}_n$ . For a particle located precisely at the BC site the hyperfine interaction has axial symmetry with respect to the [1 1 1] axis and thus  $\mathbf{A}_p$  has the form

$$\mathbf{A}_p = A_p \begin{pmatrix} 0 & 1 & 1 \\ 1 & 0 & 1 \\ 1 & 1 & 0 \end{pmatrix}, \quad (2.21)$$

with  $A_p$  being the anisotropic hyperfine parameter at this site. For a particle located precisely at the T site, all elements of  $\mathbf{A}_p$  are zero and hence the hyperfine tensor is purely isotropic.

In reality the muon/proton will explore the environment around these sites by virtue of its zero-point motion and thermal effects. In order to account for the zero-point motion the hyperfine interaction tensor must be averaged over the squared modulus of the muon/proton wave function:

$$\langle \mathbf{A} \rangle_\mu = \int |X(\mathbf{r}_\mu; \mathbf{r}_n)|^2 \mathbf{A}(\mathbf{r}_\mu) d\mathbf{r}_\mu. \quad (2.22)$$

To evaluate the integral for each component of  $\mathbf{A}$  we fit  $A_s(x_\mu, y_\mu, z_\mu)$  and each of the six distinct elements of the symmetric tensor  $\mathbf{A}_p(x_\mu, y_\mu, z_\mu)$  to polynomial expressions of the correct symmetry. Since the muon/proton wave function is expanded in terms of Hermite polynomials, analytic expressions for the elements of  $\langle \mathbf{A} \rangle_\mu$  may be obtained.

For the isotropic hyperfine parameters the polynomial expression for  $A_s(x_\mu, y_\mu, z_\mu)$  has the same symmetry as the relevant potential energy surface. These parameters were expanded in sixth-order polynomials. The polynomial describing the isotropic superhyperfine parameter at the BC site contains terms which are odd in  $z_\mu$ . (Superhyperfine parameters were not calculated for the T site.) Each of the elements of  $\mathbf{A}_p^T$  and  $\mathbf{A}_p^{BC}$  were fitted to second-order polynomials of the correct symmetry.

We now consider the symmetry of the hyperfine tensor including the effects of zero-point motion. Within the double adiabatic approximation the muon motion is described by the wave function  $X(\mathbf{r}_\mu; \mathbf{r}_n)$ . The motion-average of the  $\alpha\beta$ -component ( $\alpha, \beta = x, y, z$ ) of the anisotropic hyperfine tensor is given by:

$$\langle A_{\alpha\beta} \rangle_\mu = C \int \int |X(\mathbf{r}_\mu; \mathbf{r}_n)|^2 \rho_\sigma(\mathbf{r} + \mathbf{r}_\mu) T_{\alpha\beta}(\mathbf{r}) d\mathbf{r} d\mathbf{r}_\mu, \quad (2.23)$$

where  $C$  is a constant,  $\rho_\sigma$  is the electron spin density, and  $T_{\alpha\beta}$  denotes the components of the tensor  $\mathbf{T}$  defined in Eq. 2.20.

The muon/proton may be said to be trapped in a potential well if its wave function is negligibly small outside of an equi-potential-energy surface enclosing the region. The muon wave function,  $X$ , is the non-degenerate ground state of the potential well and therefore has the full point-group symmetry of the well, *i.e.*,

$$P(Q_i)X(\mathbf{r}_\mu; \mathbf{r}_n) = X(\mathbf{R}_i^{-1}\mathbf{r}_\mu; \mathbf{r}_n) = X(\mathbf{r}_\mu; \mathbf{r}_n), \quad (2.24)$$

where  $P$  is a scalar transformation operator,  $Q_i$  is an operation of the point group of the well, and  $\mathbf{R}_i$  is the corresponding transformation matrix. The electron spin density,  $\rho_\sigma(\mathbf{r} + \mathbf{r}_\mu)$ , satisfies

$$P(Q_i)\rho_\sigma(\mathbf{r} + \mathbf{r}_\mu) = \rho_\sigma(\mathbf{R}_i^{-1}(\mathbf{r} + \mathbf{r}_\mu)) = \rho_\sigma(\mathbf{r} + \mathbf{r}_\mu). \quad (2.25)$$

$\langle A_{\alpha\beta} \rangle_\mu$  is unchanged by a scalar transformation of the integrand, *i.e.*,

$$\langle A_{\alpha\beta} \rangle_\mu = C \int \int P(Q_i) [|X(\mathbf{r}_\mu; \mathbf{r}_n)|^2 \times \rho_\sigma(\mathbf{r} + \mathbf{r}_\mu) T_{\alpha\beta}(\mathbf{r})] d\mathbf{r} d\mathbf{r}_\mu. \quad (2.26)$$

$\langle A_{\alpha\beta} \rangle_\mu$  is again unaltered if we sum over the  $i$  operations and divide by their number,  $N$ ,

$$\langle A_{\alpha\beta} \rangle_\mu = \frac{C}{N} \sum_i \int \int P(Q_i) [|X(\mathbf{r}_\mu; \mathbf{r}_n)|^2 \times \rho_\sigma(\mathbf{r} + \mathbf{r}_\mu) T_{\alpha\beta}(\mathbf{r})] d\mathbf{r} d\mathbf{r}_\mu. \quad (2.27)$$

Using Eqs. 2.24 and 2.25 we have

$$\langle A_{\alpha\beta} \rangle_\mu = \frac{C}{N} \int \int |X(\mathbf{r}_\mu; \mathbf{r}_n)|^2 \rho_\sigma(\mathbf{r} + \mathbf{r}_\mu) \times \left[ \sum_i P(Q_i) T_{\alpha\beta}(\mathbf{r}) \right] d\mathbf{r} d\mathbf{r}_\mu. \quad (2.28)$$

The symmetry properties of  $\langle A_{\alpha\beta} \rangle_\mu$  are easily obtained from Eq. 2.28. For example,  $\langle A_{xy} \rangle_\mu$  will be equal to  $\langle A_{yz} \rangle_\mu$  if  $\sum_i P(Q_i) xy = \sum_i P(Q_i) yz$ . Taking the specific case of the T site, it is easily shown that  $\sum_i P(Q_i) xy = \sum_i P(Q_i) yz = 0$ , where the sum is over the 24 operations of the tetrahedral point group. Similar arguments show that all the elements of  $\langle A_{\alpha\beta} \rangle_\mu$  are zero for the T site. Similarly, for the BC site we find that all off-diagonal elements of  $\langle A_{\alpha\beta} \rangle_\mu$  are equal, and the diagonal elements are zero.

If the zero-point motion of the muon is neglected then  $|X(\mathbf{r}_\mu; \mathbf{r}_n)|^2 = \delta(\mathbf{r}_\mu - \mathbf{r}_0)$ , where  $\mathbf{r}_0$  is the position of the muon. It follows that if the muon is placed at an invariant point of the symmetry group of the well, then including the zero-point motion does not change the symmetry of the anisotropic hyperfine tensor. This result explains why the zero-point motion does not affect the symmetry of the anisotropic hyperfine tensor for either the T or BC sites considered here.

The presence of the muon could lead to a symmetry lowering distortion of the host lattice, in which case the appropriate point group is the lower symmetry one. We have not considered the possibility of symmetry lowering distortions in our calculations because of the computational cost of evaluating the energy  $E^e(\mathbf{r}_\mu, \mathbf{r}_n)$  of Eq. 2.2 for the required atomic configurations. However, we believe such distortions to be unlikely for the cases considered here.

### III. RESULTS

#### A. Static relaxations

The static relaxations (neglecting zero-point motion) are, of course, identical for the muon and proton. Calculations with the muon/proton fixed at the BC site of the 16-atom silicon cell showed that the two nearest neighbours of the muon/proton relax outwards from the muon/proton by 0.40 Å along the [1 1 1] axis with the NNNs relaxing by 0.01 Å in the same direction. The corresponding relaxations for the 54-atom supercell were 0.39 Å and 0.02 Å. These values are close to the plane-wave pseudopotential results of Luchsinger *et al.* [7] who obtained relaxations of 0.45 Å for the NN silicon atoms and 0.07 Å for the NNNs. For the 16-atom germanium

cell the corresponding relaxations were 0.44 Å for the NNs and 0.02 Å for the NNNs. Our NN relaxation is in good agreement with the value of 0.42 Å calculated by Vogel *et al.* [24]

At the T site, the NN atoms in the host lattice were allowed to relax in the radial direction. The relaxations in silicon and germanium were approximately equal and very small; just 0.02 Å *towards* the muon/proton in the 16-atom supercell and 0.03 Å (in the same direction) in the 54-atom supercell. Again, this is in agreement with the “negligible” relaxation for the T site in silicon found by Luchsinger *et al.*

## B. Relaxations including zero-point motion

The influence of the zero-point motion of the muon/proton on the relaxation of the silicon/germanium host lattice was studied by calculating the total energy,  $E_\alpha^n$ , of Eq. 2.4, for different relaxations of the NN host atoms, as described in Section II C.

For the BC site four different relaxations of the NNs were considered, and for each of these the six NNNs were also relaxed. The NN relaxations are in addition to the static relaxations given in Section III A. The inclusion of the zero-point energy of the muon was found to give only a small correction to the static relaxations; the NN silicon atoms relaxed outwards by just an additional 0.01 Å in the [1 1 1] direction, so that the final separation of the muon from a NN silicon atom is 1.58 Å in the 16-atom supercell. The much smaller zero-point energy of the heavier hydrogen impurity is swamped by the increase in energy of the crystal as the separation of the NN atoms is increased and thus there is no additional relaxation. As a check on the finite-size errors, the energies of five geometries were recalculated using the 54-atom supercell. These energies and the corresponding potential energy curves calculated within the 16-atom supercell are shown in Fig. 2. The very small differences between the 16-atom and 54-atom results justify the use of the 16-atom supercell in calculations of the shape of the potential well at the BC site.

The story is very similar for the BC site in germanium. When the zero-point energy of the muon is included, the relaxation of the NN atoms again increases by just 0.01 Å, so that the final separation of the muon from a NN germanium atom is 1.69 Å in the 16-atom supercell. Once more, the smaller zero-point energy of the proton means there is no additional relaxation due to quantum effects. Fig. 3 shows the potential energy well and calculated wave functions for the muon and proton at the BC site in germanium.

## C. Zero-point energies

The zero-point energy of the muon at the BC site was calculated to be 0.63 eV in silicon and 0.56 eV in germanium. It is perhaps surprising that such large zero-point energies have so little effect on the relaxations. As shown in Fig. 4, the potential well is narrow in the direction along the bond and wider perpendicular to the bond. Within the harmonic approximation one can decompose the zero-point energy into contributions from the well along and perpendicular to the bond. For a muon at the BC site in silicon this gives 0.47 eV in the direction along the bond and 0.22 eV perpendicular to the bond. (The sum of these differs from the full zero-point energy of 0.63 eV because the latter does not assume the harmonic approximation.) The corresponding energies for germanium are 0.37 eV and 0.22 eV in the directions along and perpendicular to the bond, respectively. If we were to consider only the zero-point energy in the direction along the bond then the outwards relaxation of the silicon/germanium atoms would be larger; approximately 0.03 Å in silicon and more than 0.025 Å in germanium. Although the component of the zero-point energy along the bond is significantly reduced by further outward relaxation of the silicon/germanium atoms, the potential well also gets narrower in the plane perpendicular to the bond, which tends to increase the zero-point energy. The narrowing of the potential well in the plane perpendicular to the bond correlates with the narrowing of the bonding charge cloud as the bond lengthens.

Our result of 0.63 eV for the zero-point energy of the muon at the BC site in silicon is close to the value of 0.54 eV obtained by Claxton *et al.* [25] from Hartree-Fock calculations on  $\text{Si}_{26}\text{H}_{30}$  clusters. In that calculation the potential well at the BC site was assumed to be cylindrically symmetric about the bond (as it is in this work) and the resulting Schrödinger equation was solved within the harmonic approximation.

The larger mass of the proton significantly reduces the quantum effects. We calculated the zero-point energy of a proton at the BC site to be 0.20 eV in silicon and 0.18 eV in germanium. Our value for silicon is close to that of 0.18 eV obtained by Luchsinger *et al.* [7], which suggests that the harmonic approximation to the potential well used in that work is quite good for the proton ground state.

In contrast to the results of plane-wave pseudopotential calculations [7,28], we find the T site corresponds to a local minimum in the potential energy surface. This is, however, in agreement with a more recent plane-wave pseudopotential study. [29] The calculated energy surface along the [1 1 1] direction is shown in Fig. 5. It turns out that the muon/proton is not strongly bound in our potential well, which turns over at the hexagonal site situated at a distance of 1.18 Å from the T site along the [1 1 1] direction. To confine the muon/proton in the well we therefore constrained the fit to prevent the potential

turning over, as shown in Fig. 5. The zero-point energy of the muon/proton calculated in such a well is then an upper bound on the true value, but as the wave function decays quite rapidly away from the T site this bound is accurate.

In contrast to the BC site, investigation of the finite size effects present in the calculation of this energy surface showed that while the results in the 16- and 54-atom supercells were qualitatively similar, they differed significantly in the openness and depth of the potential well. As a result, the calculation of the zero-point energy *etc.* of the muon/proton at this site was carried out using the potential well obtained from the 54-atom supercell. The expense of the LSDA calculations with this supercell made the generation of data points off the  $[1\ 1\ 1]$  axis too costly. Therefore, the three parameters left undetermined after the one-dimensional fit to the data on the  $[1\ 1\ 1]$  axis were assigned the values obtained in the fit to the 16-atom supercell data. This is not a critical choice since the one-dimensional fit has already constrained the shape of the energy surface in eight directions (due to the symmetry of the T site). This procedure was also used to generate a three-dimensional potential-energy function from the fit to data along the  $[1\ 1\ 1]$  axis (calculated using the 16-atom supercell) at the T site in germanium. The parameters obtained from these fits are given in Table II.

For a muon at the T site the zero-point energy was calculated to be 0.28 eV in silicon and 0.22 eV in germanium. For a proton the corresponding values are 0.09 eV and 0.06 eV. The ground state wave functions of the muon/proton along the  $[1\ 1\ 1]$  axis in silicon are shown in Fig. 5 and those in germanium in Fig. 6. The results for germanium must be considered approximate since we have not calculated any data points off the  $[1\ 1\ 1]$  axis in this case. In addition, the 16-atom supercell was used for all of the germanium calculations and therefore it follows from the behaviour found in silicon that the true potential energy surface will be more open than the one we have obtained.

#### D. Excited states of the muon and proton

For a muon at the BC site in silicon our zero-point energy of 0.63 eV is considerably smaller than the well depth of 1.37 eV, indicating the possibility that excited states of the muon may be bound within the well. Numerical calculations show a two-fold degenerate first excited state at an energy of 0.84 eV. The wave functions of these states are similar to those obtained from a harmonic approximation, *i.e.*, they consist essentially of an excitation within the plane perpendicular to the bond. The energy of the first excited state is also reasonably well described within the harmonic approximation which predicts the excited state to be 0.22 eV above the ground state. It is also possible that some of the higher energy states are

bound within the well. In germanium, the potential well at the BC site is 1.51 eV deep. The first excited state is two-fold degenerate with an energy of 0.78 eV and is of the same character as in silicon.

For the more massive proton the excited states are of lower energy. At the BC site in silicon, the two-fold degenerate first excited state of the proton has an energy of 0.27 eV, which is 0.07 eV higher than the ground state, while in germanium the excited state has an energy of 0.25 eV, which is also 0.07 eV above the ground state.

Each excited state of the muon/proton defines a different adiabatic potential for the nuclei (*i.e.*, a different  $E_\alpha^\mu(\mathbf{r}_n)$  in Eq. 2.7). It is therefore possible for the lattice relaxations that occur when the muon/proton is in its first excited state (say) to be different from those for the ground state. For instance, the fact that the wave function of the first excited state of the muon/proton is essentially an excitation in the plane perpendicular to the bond, combined with the fact that the potential well in this plane becomes narrower as the separation of the NN atoms increases, results in the NN atoms actually relaxing towards the impurity. This relaxation is small for the muon, but effectively zero for the proton due to the smaller zero-point energy. The effect on the energies of the excited states is negligible.

At the T site in silicon, the potential well is considerably shallower with a depth of only 0.20 eV. For the muon this means that even the ground state energy (0.28 eV) of our constrained potential well (which is an upper bound on the true ground state energy) is greater than the well depth. The proton, however, has a (triply degenerate) first excited state with an energy of 0.14 eV which may therefore be bound at the T site. In germanium the potential well at the T site has a depth of just 0.18 eV in our 16-atom supercell calculations. It follows from the behaviour found in going from the 16-atom to the 54-atom supercell in silicon that the true well depth in germanium will probably be less than this. It is therefore unlikely that excited states of either the muon or the proton will be bound at the T site in germanium.

#### E. Energy barriers at the T and BC sites

The heights of the energy barriers confining the muon and proton at the BC and T sites are clearly of great importance in determining the dynamics of the impurities within the lattice and hence are a significant part of the configuration-coordinate diagram.

The static barriers (*i.e.*, excluding zero-point effects) experienced by the muon and proton are identical. For the BC site in silicon we calculate the static barrier to motion towards the hexagonal site (in the  $[-1\ 1\ 0]$  direction) to be 1.37 eV while in germanium it is 1.51 eV. The effective barrier height is reduced by the zero-point energy and therefore depends on the nature of the impurity. Including this effect, the effective barrier experi-



enced by a muon at the BC site in silicon is 0.74 eV while in germanium it is 0.95 eV. For the proton, the effective barriers (1.17 eV in silicon and 1.33 eV in germanium) are higher. The effective barrier height for the muon at the BC site may be considered a measure of the barrier to the BC→T site transition. In reality this transition is believed to involve charged states: muonium at the BC site is first ionized (with activation energy 0.22 eV [30]) and then moves to the T site while simultaneously recapturing an electron to regain its neutral charge state. The sum of the activation and barrier energies for these two processes as measured experimentally is 0.60 eV. [30]

At the T site the energy barriers are very much lower. In silicon the static barrier to motion of the muon towards the hexagonal site (in the [1 1 1] direction) is calculated to be 0.20 eV while in germanium it is 0.18 eV. When zero-point effects are taken into account, the effective barriers for the muon at the T site in silicon and germanium are zero indicating that, even at  $T = 0\text{K}$ , the muon is free to diffuse through the interstitial region. However, this barrier is not appropriate for the T→BC site transition because in our calculations for the muon in the interstitial region, the host atoms around the BC site are unrelaxed. The process by which these atoms relax the large distances required to allow the muon to move to the BC site is unclear. Experimentally, the barrier for the T→BC site transition in silicon is 0.39 eV. [30]

Since the zero-point energy of the proton is around a third of that of the muon, these calculations indicate that it will be bound at the T site in both silicon and germanium with an effective barrier of around 0.12 eV in each case. As previously discussed the true effective barrier in germanium will probably be lower than this.

## F. Hyperfine and superhyperfine parameters

The hyperfine parameters depend on the spin density in the region at and around the atomic nuclei. More specific insight into the origin of the large measured differences between hyperfine parameters for muons located at the two impurity sites can be gained from a consideration of the spin density isosurfaces. Fig. 7 shows spin density contour plots for silicon in appropriate planes encompassing the BC and T sites. Evidently the majority spin density around an impurity placed at the BC site is largely dispersed onto the two nearest-neighbour silicon atoms; the spin density in a small region around the hydrogen nucleus is comparatively small and of opposite sign. At the T site, by contrast, almost all of the majority spin density is localized on the defect. From these calculations one therefore expects the isotropic hyperfine parameter at the two sites to be of opposite sign, with the magnitude of the parameter at the BC site much smaller than at the T site.

It is of course necessary to check the dependence of calculated hyperfine and superhyperfine parameters on the

supercell size and basis set quality. A set of computed numbers are shown in Table III. The parameters appear to be reasonably well converged with respect to the basis set, but the convergence with increasing supercell size is less good, particularly for the isotropic hyperfine and superhyperfine parameters at the BC site. Table IV gives the hyperfine and superhyperfine parameters calculated at the BC site in both silicon and germanium together with the results of other calculations for comparison. Without motion averaging, the values obtained for silicon using the LSDA approximation are in reasonable agreement with both experiment and other DFT calculations.

Both the hyperfine and superhyperfine motion-averaged tensors ( $\langle \mathbf{A}_{p\mu}^{\text{BC}} \rangle$  and  $\langle \mathbf{A}_{p\text{Si}}^{\text{BC}} \rangle$ ) were found to be axially symmetric about the Si–Si bond ([1 1 1] direction) in agreement with the experimental results. As Luchsinger *et al.* [7] found, motion averaging increases the values of all but one (the anisotropic hyperfine parameter) of the hyperfine and superhyperfine parameters, with the isotropic (contact) term on the muon being the most sensitive. This is because of the very small contact charge density which varies quite significantly with the muon position (Fig. 8). In agreement with Luchsinger *et al.* [7], use of the Perdew–Wang [16] GGA functional did not consistently improve the values of the parameters. The results obtained for the muon at the BC site in germanium follow a similar pattern.

The calculated hyperfine parameters for the T site are given in Table V. For silicon our values are in good agreement with both experiment and previous calculations. Again use of the Perdew–Wang [16] GGA functional fails to improve this agreement. For germanium, our value of the isotropic hyperfine parameter at the T site also agrees quite well with the measured value.

The behaviour of the isotropic hyperfine parameter along the [1 1 1] axis in the vicinity of the T site in silicon and germanium is shown in Fig. 9. Motion averaging for the muon/proton at the T site reduces the isotropic hyperfine parameter in both silicon and germanium. The final motion-averaged results are in reasonable agreement with experiment. Motion averaging of  $\mathbf{A}_{p\mu}^{\text{T}}$  resulted in an isotropic tensor, in agreement with the symmetry arguments presented in Section IID and experimental observations.

In a recent application of the path-integral Monte Carlo approach, Miyake *et al.* [11] studied hydrogen and muonium at the T site in silicon, with the electron–electron interactions calculated within the LDA. They found the T site to be a local maximum in the potential energy surface, in agreement with Luchsinger *et al.* [7] but in disagreement with our results and a recent plane-wave pseudopotential calculation. [29] Their path-integral Monte Carlo study showed that quantum effects led to the muonium distribution being centred on the T site while hydrogen behaved as a largely classical particle and was thus distributed away from the local maximum

on that site. Evaluating the motion-averaged isotropic hyperfine parameter with our hyperfine data gives a value of 492 MHz for the hydrogen distribution of Miyake *et al.*, but 685 MHz with our hydrogen distribution. Therefore if one could measure the isotropic hyperfine signal of *hydrogen* at the T site, one could deduce whether the T site is a maximum or minimum in the potential energy surface.

### G. Energies of a muon/proton at the T and BC sites

The question of the relative stabilities of the muon and proton at the BC and T sites is of considerable interest. For a particular impurity this energy difference is the sum of contributions from the static-lattice energy and the zero-point energy. The contribution from the static lattice is sensitive to the size of the supercell and to the quality of the basis set. We investigated this point using the 16- and 54-atom supercells. We have added a BSSE correction to each of the static-lattice energy differences quoted here. With the 16-atom silicon cell and the standard basis set, the T site was found to be 0.63 eV lower in energy than the BC site. Using the large basis set reduced this to 0.32 eV. In the 54-atom supercell and using the standard basis set the T site was 0.41 eV lower in energy than the BC site. With the large basis set, this was reduced to just 0.07 eV. These results indicate that a 16-atom supercell is too small to give reliable estimates of the static-lattice energy difference between the two sites. A summary of the computed energies that influence the relative stabilities is given in Table VI.

There have been several previous calculations of the static-lattice energy difference between the T and BC sites in silicon. Using a plane-wave pseudopotential method and the LSDA, Chang and Chadi [8] found the T site to be lower in energy, but only by an amount  $\leq 0.25$  eV. Luchsinger *et al.* [7], also using a plane-wave pseudopotential method, found the T site to be 0.15 eV higher in energy than the BC site within the LSDA and 0.19 eV higher within the GGA. Note, however, that Luchsinger *et al.* [7] found the T site to be a local maximum in the energy and that a nearby site has an energy about 0.05 eV lower. It is clear from the various results that the static-lattice energy difference between the T and BC sites in silicon is small within the LSDA/GGA, but its precise value has yet to be settled.

The fact that the static-lattice energy difference is small means that the zero-point energy of the impurity is crucial in determining the relative stability of the T and BC sites. For a muon in silicon we have found the zero-point energy at the BC site to be 0.35 eV larger than at the T site. This difference is large enough to to make the BC site unfavourable for the muon, irrespective of which of the above values for the static-lattice energy difference is used. However, the zero-point energy of the proton at the BC site in silicon is only 0.12 eV higher

than at the T site. Therefore, for this impurity the relative stability of the two sites depends on the precise value of the static-lattice energy difference.

In germanium with a 16-atom supercell, the difference in static lattice energies favours the T site by an energy of 0.57 eV. The convergence with respect to supercell size found in silicon suggests that this difference in a fully converged LSDA calculation would be smaller. We estimate that the zero-point energy of a muon at the BC site is 0.34 eV larger than at the T site (where the form of the potential energy surface was obtained from data calculated along the  $[1\ 1\ 1]$  axis only). For a proton the corresponding value is 0.12 eV. These results are similar to those obtained in silicon and thus it is likely that for the muon the T site is lower in energy. Without a fully converged value for the static lattice energy difference we are unable to draw any conclusions on the lowest energy site of the proton.

## IV. CONCLUSIONS

We have calculated the zero-point motions and energies as well as the hyperfine parameters of both muonium and hydrogen when present as impurities in silicon and germanium crystals at the BC and T sites. The electron, muon/proton and ion motions were decoupled using a double adiabatic approximation, and for the BC site we have included the effect of the zero-point motion on the relaxation of the host lattice. The ground states of both the muon and proton at the BC sites of silicon and germanium are strongly confined within a potential well of depth 1.37 eV (silicon) and 1.51 eV (germanium). The zero-point energy of a muon at the BC site is calculated to be 0.63 eV for silicon and 0.56 eV for germanium. Despite the relatively large zero-point energy of the muon at the BC site, it causes only a small additional outwards relaxation of the nearest-neighbour silicon/germanium atoms of about 0.01 Å. For the proton the additional relaxations of the nearest neighbours due to zero-point motion are negligible. At the T site the static relaxations of the host atoms are very small and the zero-point energy is considerably smaller than at the BC site, being 0.28 eV (0.22 eV) for a muon in silicon (germanium). It is therefore reasonable to assume that the additional relaxation due to the zero-point motion is negligible for either a muon or proton at the T site.

The relaxation of the crystal around either the BC or T sites is practically independent of whether the impurity is a muon or a proton. This result confirms one of the underlying assumptions of the widely accepted configuration coordinate model. [3] The potential well at the BC sites of both silicon and germanium is reasonably well described by a harmonic approximation, at least for the ground states of the muon and proton. The potential well at the BC site in both materials is deep enough to bind several excited states of the muon and proton, although

we are not aware of any experimental evidence for such states. The potential well at the T site in either silicon or germanium is not deep enough to bind the muon which is free to diffuse through the interstitial region, although our calculations suggest that the proton is bound at this site at  $T = 0$  K.

Various LSDA and GGA calculations have indicated that the energies for a static muon or proton at the BC and T sites in silicon are very similar. However, we have calculated the difference in zero-point energies of a muon at the T and BC sites in silicon (germanium) to be 0.35 eV (0.34 eV) which is sufficient to make the T site more stable, whether we assume our value for the static-lattice energy difference between the BC and T sites or those of others. [8,7] This result is in conflict with the interpretation of experimental data.

The hyperfine parameters calculated for silicon in our all-electron calculations are close to those obtained in plane-wave pseudopotential calculations. This agreement confirms that the procedure used to correct for the pseudopotential and for the incomplete plane-wave basis sets are accurate. For silicon our static LSDA results are in reasonable agreement with other LSDA results and experiment. Our hyperfine parameter for the muon at the T site in germanium is in much better agreement with experiment than the only previous calculation of which we are aware. [27]

In our work the motion averages of the hyperfine and superhyperfine parameters are evaluated by averaging over the squared modulus of the wave function obtained from the full solution of the muon/proton Schrödinger equation in the potential well. We note that the symmetry of the potential wells requires that the symmetry of the motion-averaged hyperfine tensors at the T and BC sites are the same as if the muon/proton was situated exactly at the sites. We have obtained detailed information about the variation of the hyperfine and superhyperfine parameters with the position of the muon/proton. Our results show that motion averaging for the muon/proton at the BC site in silicon and germanium increases the values of all of the hyperfine and superhyperfine parameters apart from the anisotropic hyperfine term which decreases slightly, in agreement with the conclusions of Luchsinger *et al.* [7] With the exception of the isotropic hyperfine term however, all of the changes are small. At the T sites in silicon and germanium, motion averaging reduces the isotropic hyperfine parameter.

## V. ACKNOWLEDGMENTS

We thank R. Q. Hood and M. I. J. Probert for useful discussions. Financial support was provided by the Engineering and Physical Sciences Research Council (UK).

- [1] B. D. Patterson, *Rev. Mod. Phys.* **60**, 69 (1988).
- [2] M. C. R. Symons, *Hyp. Int.* **17-19**, 771 (1984); S. F. J. Cox and M. C. R. Symons, *Chem. Phys. Lett.* **126**, 516 (1986).
- [3] R. L. Lichti, *Phil. Trans. R. Soc. Lond. A* **350**, 323 (1995); S. R. Kreitzman *et al.*, *Phys. Rev. B* **51**, 13117 (1995); S. F. J. Cox, *Phil. Trans. R. Soc. Lond. A* **350**, 171 (1995).
- [4] R. G. Parr and W. Yang, *Density Functional Theory of Atoms and Molecules* (Oxford University Press, 1989).
- [5] C. G. Van de Walle, *Phys. Rev. Lett.* **64**, 669 (1990).
- [6] C. G. Van de Walle and P. E. Blöchl, *Phys. Rev. B* **47**, 4244 (1993).
- [7] R. H. Luchsinger, Y. Zhou, and P. F. Meier, *Phys. Rev. B* **55**, 6927 (1997).
- [8] K. J. Chang and D. J. Chadi, *Phys. Rev. B* **40**, 11644 (1989).
- [9] R. P. Feynman and A. R. Hibbs, *Quantum Mechanics and Path Integrals* (McGraw-Hill, New York, 1965).
- [10] R. Ramírez and C. P. Herrero, *Phys. Rev. Lett.* **73**, 126 (1994).
- [11] T. Miyake, T. Ogitsu and S. Tsuneyuki, *Phys. Rev. Lett.* **81**, 1873 (1998).
- [12] R. Dovesi, V. R. Saunders, C. Roetti, M. Causà, N. M. Harrison, R. Orlando, and E. Aprà, *CRYSTAL95 User Manual*, Università di Torino and CCLRC Daresbury Laboratory (1996).
- [13] P. Hohenberg and W. Kohn, *Phys. Rev.* **136**, B864 (1964).
- [14] W. Kohn and L. J. Sham, *Phys. Rev.* **140**, A1133 (1965).
- [15] J. P. Perdew and A. Zunger, *Phys. Rev. B* **23**, 5048 (1981) who parameterized the diffusion quantum Monte Carlo data for the homogeneous electron gas calculated by D. M. Ceperley and B. J. Alder, *Phys. Rev. Lett.* **45**, 566 (1980).
- [16] J. P. Perdew and Y. Wang, *Phys. Rev. B* **33**, 8800 (1986).
- [17] C. Pisani, R. Dovesi and C. Roetti, *Hartree-Fock Ab Initio Treatment of Crystalline Systems* (Springer Verlag, Berlin, 1988), Vol. 48.
- [18] H. J. Monkhorst and J. D. Pack, *Phys. Rev. B* **13**, 5188 (1976).
- [19] M. F. Guest and V. R. Saunders, *Mol. Phys.*, **28**, 819 (1974) ; E. Clementi, ed. *MOTEC91*, ESCON, Leiden (1991).
- [20] <http://www.tcm.phy.cam.ac.uk/~mdt26/crystal.html>, TCM CRYSTAL basis set library, M.D. Towler (1998).
- [21] S. F. Boys and J. Bernardi, *Mol. Phys.*, **19**, 553 (1970).
- [22] The nuclear  $g$  factor is related to the gyromagnetic ratio,  $\gamma^n$ , through the relation  $g_n\mu^n = \gamma^n$  [MHz/T].
- [23] The values of the fundamental constants used to calculate the prefactor in the expression for  $A_s$  as well as the values of  $\gamma^n$  for the muon and proton were taken from E. R. Cohen and B. N. Taylor, *The Fundamental Physical Constants*, *Physics Today*, August 1994.
- [24] S. Vogel, M. Celio, Dj. M. Maric and P. F. Meier, *J. Phys. Cond. Matt.* **1**, 4729 (1989).
- [25] T. A. Claxton, Dj. M. Maric and P. F. Meier, *Chem. Phys. Lett.* **192**, 29 (1992).
- [26] R. F. Kiefl and T. L. Estle, in *Hydrogen in Semiconductors*, edited by J. I. Pankove and N. M. Johnson, *Semi-*

*conductors and Semimetals* Vol. 34 (Academic, Boston, 1991), p. 547.

- [27] M. Casarin, G. Granozzi, E. Tondello and A. Vittadini, *Chem. Phys.* **154**, 385 (1991).
- [28] C. G. Van de Walle, P. J. H. Denteneer, Y. Bar-Yam, and S. T. Pantelides, *Phys. Rev. B* **39**, 10791 (1989).
- [29] M. I. J. Probert, private communication.
- [30] S. R. Kreitzman, B. Hitti, R. L. Lichti, T. L. Estle, and K. H. Chow, *Phys. Rev. B* **51**, 13117 (1995).

TABLE I. The values of the parameters in Eq. 2.8 defining the potential well at the BC site of silicon and germanium. The fit is applicable within a cylinder centred on the BC site of radius 1.0 Å (1.1 Å) in the plane perpendicular to the bond and up to  $\pm 0.5$  Å (0.37 Å) along the direction of the bond in silicon (germanium). The units are such that if the lengths in Eq. 2.8 are expressed in Bohr radii then the potential energy is in Ha. N.B. The values quoted are those carried into the zero-point calculation and therefore the number of significant figures should not be taken as an indication of the accuracy of the fit.

|          | Silicon     | Germanium   |
|----------|-------------|-------------|
| $\beta$  | 0.00588753  | 0.00610711  |
| $\gamma$ | 0.0807689   | 0.0548517   |
| $\delta$ | 0.0         | 0.0         |
| $\zeta$  | 0.000337036 | 0.000224779 |
| $\eta$   | 0.0654643   | 0.0506238   |

TABLE II. The parameters defining the expansions (Eq. 2.9) of the potential energy surface around the T site in silicon and germanium. The fit is applicable over the region bounded by a sphere of radius 1.0 Å centred on the T site. The units are such that if the lengths in Eq. 2.9 are expressed in Bohr radii then the potential energy is in Ha. N.B. The values quoted are those carried into the zero-point calculation and therefore the number of significant figures should not be taken as an indication of the accuracy of the fit.

|       | Silicon      | Germanium    |
|-------|--------------|--------------|
| $a_2$ | 0.00440492   | 0.00151269   |
| $a_3$ | 0.00589898   | 0.00542489   |
| $a_4$ | -0.00197527  | 0.000339949  |
| $b_4$ | 0.000930883  | -0.000160207 |
| $a_5$ | -0.00456177  | -0.00311144  |
| $a_6$ | 0.00155753   | 0.000775975  |
| $b_6$ | -0.000556122 | -0.000277064 |
| $c_6$ | 0.00696501   | 0.00347002   |

TABLE III. The dependence of hyperfine and superhyperfine parameters for muonium in silicon on supercell size and basis set.

| Supercell | Basis set | BC site     |             |                     |                     | T site      |
|-----------|-----------|-------------|-------------|---------------------|---------------------|-------------|
|           |           | $A_{s_\mu}$ | $A_{p_\mu}$ | $A_{s_{\text{Si}}}$ | $A_{p_{\text{Si}}}$ | $A_{s_\mu}$ |
| 16 atom   | Standard  | -27.1       | 17.7        | -147                | -13.6               | 2302        |
| 16 atom   | Large     | -21.4       | 13.0        | -114                | -10.7               | 2366        |
| 54 atom   | Standard  | -1.6        | 16.4        | -91.0               | -12.4               | 2362        |
| 54 atom   | Large     | 4.5         | 9.8         | -57.1               | -8.1                | 2389        |

TABLE IV. Static and motion-averaged (indicated by  $\langle \rangle$ ) hyperfine parameters for the muon at the BC site and the nearest-neighbour atoms. PS denotes a pseudopotential calculation.

|                                   | Hyperfine parameters (MHz) |             |                     |                     |             |             |                     |                     |
|-----------------------------------|----------------------------|-------------|---------------------|---------------------|-------------|-------------|---------------------|---------------------|
|                                   | Silicon                    |             |                     |                     | Germanium   |             |                     |                     |
|                                   | $A_{s_\mu}$                | $A_{p_\mu}$ | $A_{s_{\text{Si}}}$ | $A_{p_{\text{Si}}}$ | $A_{s_\mu}$ | $A_{p_\mu}$ | $A_{s_{\text{Ge}}}$ | $A_{p_{\text{Ge}}}$ |
| LSDA <sup>a</sup>                 | -1.6                       | 16.4        | -91.0               | -12.4               |             |             |                     |                     |
| LSDA <sup>b</sup>                 | -27.1                      | 17.7        | -147                | -13.6               | -24.6       | 16.4        | -80.7               | -5.8                |
| $\langle \text{LSDA} \rangle^b$   | 2.5                        | 14.5        | -141                | -13.4               | 3.6         | 12.5        | -75.5               | -5.6                |
| GGA <sup>b</sup>                  | -89.3                      | 18.9        | -155                | -14.0               | -64.6       | 17.1        | -81.0               | -5.9                |
| LSDA <sup>c</sup>                 | -104                       | 58.5        | -127                | -53.5               | -87         | 64          | -85                 | -24                 |
| PS-LSDA <sup>d</sup>              | -26                        | 22.8        | -90                 | -20.2               |             |             |                     |                     |
| PS-GGA <sup>d</sup>               | -81                        | 27.5        | -192                | -28                 |             |             |                     |                     |
| $\langle \text{PS-GGA} \rangle^d$ | -65                        | 21.7        | -191                | -26.2               |             |             |                     |                     |
| PS-LSDA <sup>e</sup>              | -26.8                      | 18.1        | -83.8               | -22.7               |             |             |                     |                     |
| PS-LSDA <sup>f</sup>              | -35                        | 22.3        | -85                 | -21.5               |             |             |                     |                     |
| Experiment <sup>g</sup>           | -67.3                      | 25.3        | -95.1               | -21.2               |             |             |                     |                     |
| Experiment <sup>h</sup>           |                            |             |                     |                     | -96.5       | 34.6        |                     |                     |

<sup>a</sup>This work, 54-atom supercell and “standard” basis set.

<sup>b</sup>This work, 16-atom supercell and “standard” basis set.

<sup>c</sup>Casarin *et al.* [27]

<sup>d</sup>Luchsinger *et al.* [7]

<sup>e</sup>Van de Walle. [5]

<sup>f</sup>Van de Walle and Blöchl. [6]

<sup>g</sup>Kiefl and Estle. [26]

<sup>h</sup>Patterson. [1]

TABLE V. Isotropic hyperfine parameters for the muon at the T site of silicon and germanium. The quoted results are for the “standard” basis set.

|                            | $A_{s_\mu}$ (MHz) |           |
|----------------------------|-------------------|-----------|
|                            | Silicon           | Germanium |
| LSDA <sup>a</sup>          | 2302              | 2236      |
| GGA <sup>a</sup>           | 2651              | 2548      |
| $\langle$ LSDA $\rangle^a$ | 2096              | 2032      |
| LSDA <sup>b</sup>          | 2362              |           |
| $\langle$ LSDA $\rangle^b$ | 2152              |           |
| PS-LSDA <sup>c</sup>       | 1939              |           |
| PS-GGA <sup>c</sup>        | 2098              |           |
| LSD-VBH <sup>d</sup>       | 3043              | 3977      |
| Experiment <sup>e</sup>    | 2006              | 2360      |

<sup>a</sup>This work, 16-atom supercell.

<sup>b</sup>This work, 54-atom supercell.

<sup>c</sup>Luchsinger *et al.* [7]

<sup>d</sup>Casarin *et al.* [27], extended basis set.

<sup>e</sup>Patterson [1] and references therein.

TABLE VI. A summary of the energies influencing the relative stability of the BC and T sites in silicon and germanium. The importance of the zero-point energy of the muon in determining the favoured site is clear.

|   | Silicon           |                    | Germanium         |                    |
|---|-------------------|--------------------|-------------------|--------------------|
|   | BC site           | T site             | BC site           | T site             |
| Static lattice energy w.r.t. BC site (eV)   | 0                 | −0.07 <sup>a</sup> | 0                 | −0.57 <sup>b</sup> |
| Muon zero-point energy (eV)                 | 0.63 <sup>c</sup> | 0.28 <sup>d</sup>  | 0.56 <sup>b</sup> | 0.22 <sup>b</sup>  |
| Total energy w.r.t. BC site for muon (eV)   | 0                 | −0.42              | 0                 | −0.91              |
| Proton zero-point energy (eV)               | 0.20 <sup>c</sup> | 0.09 <sup>d</sup>  | 0.18 <sup>b</sup> | 0.06 <sup>b</sup>  |
| Total energy w.r.t. BC site for proton (eV) | 0                 | −0.18              | 0                 | −0.69              |

<sup>a</sup>54-atom supercell and “large” basis set.

<sup>b</sup>16-atom supercell.

<sup>c</sup>16-atom supercell and “standard” basis set.

<sup>d</sup>54-atom supercell and “standard” basis set.

FIG. 1. The muon/proton at the bond-centred (a) and tetrahedral (b) sites in silicon. The dashed circles in (a) show the unrelaxed positions of the silicon atoms. These are not shown in (b) because the relaxation around the T site is negligible.

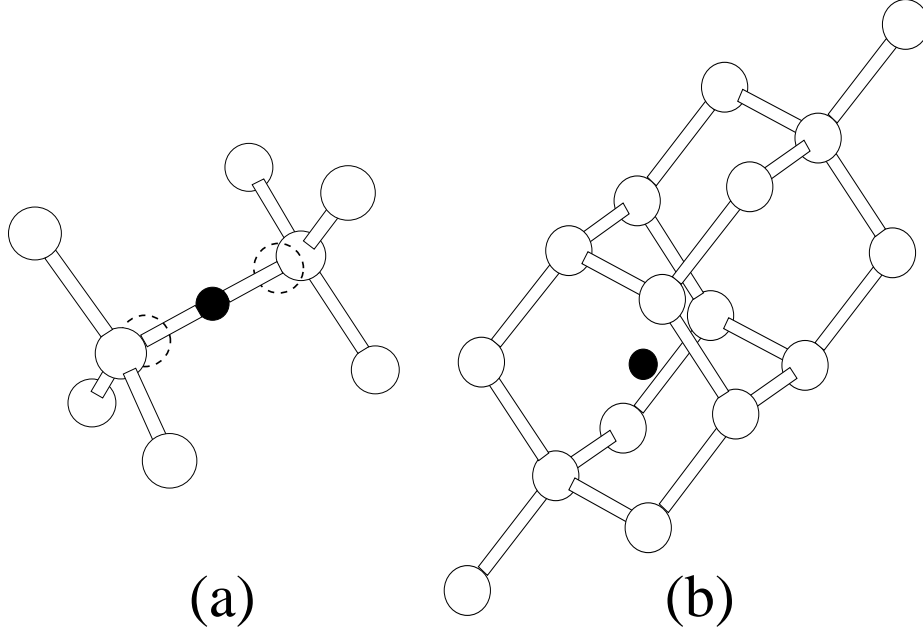


FIG. 2. The square of the proton (thin solid line) and muon (dashed line) wave functions at the BC site in silicon. The symbols denote the potential well for the 16- and 54-atom supercells, and the thick solid line is the fit of the 16-atom data to Eq. 2.8 with the parameters of Table I.

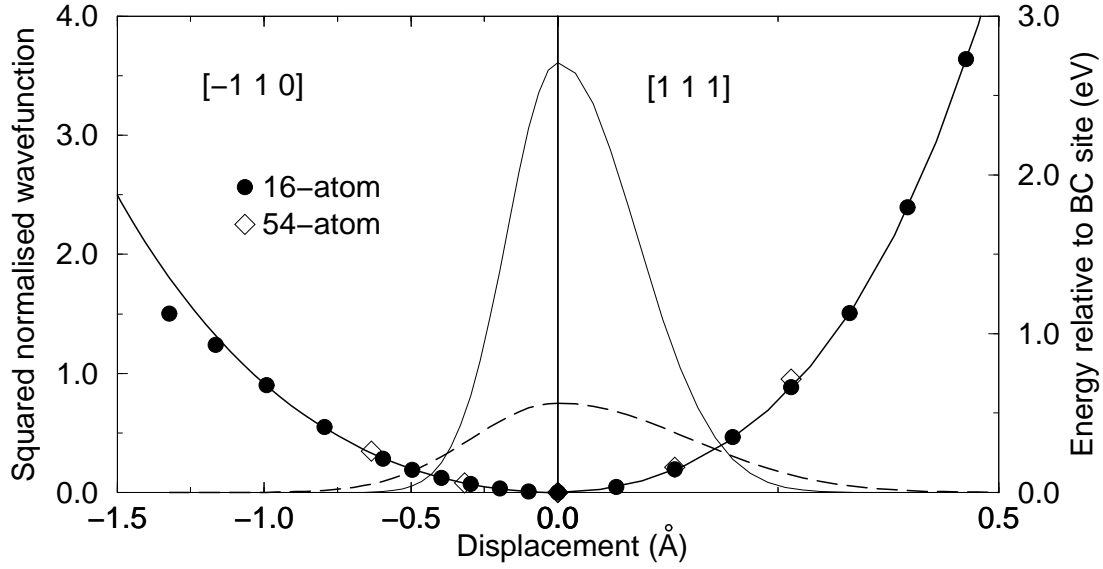


FIG. 3. The square of the proton (thin solid line) and muon (dashed line) wave functions at the BC site in germanium. The symbols denote the potential well for the 16-atom supercell, and the thick solid line is the fit to Eq. 2.8 with the parameters of Table I.

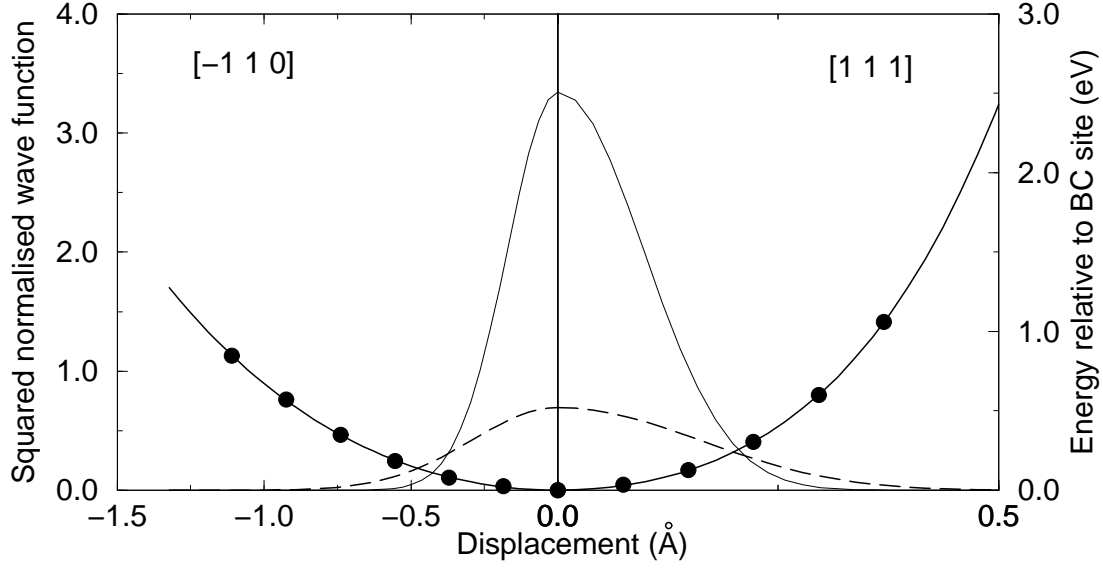


FIG. 4. The calculated potential experienced by the muon/proton in the  $\{110\}$  planes for the BC site in silicon. The figure shows both of the NN and two of the NNN silicon atoms of the muon/proton with the bond lengths drawn to scale. The contours range from 0.1 to 0.7 eV in increments of 0.1 eV.

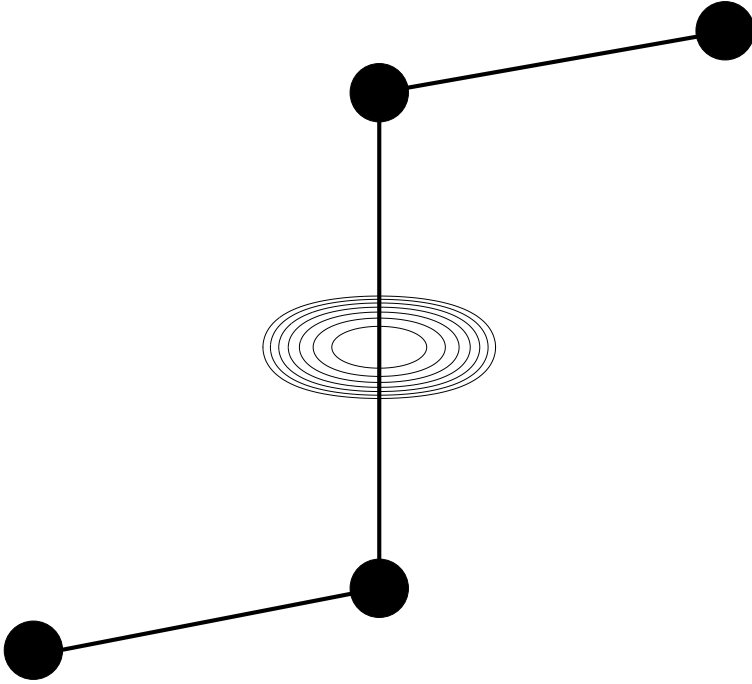




FIG. 5. The square of the proton (thin solid line) and muon (dashed line) wave functions at the T site in silicon. The symbols denote the potential well for the 54-atom supercell, and the thick solid line is the fit to Eq. 2.9 with the parameters of Table II. The potential has a maximum at the hexagonal site situated at 1.18 Å from the T site, but the fit has been constrained so that it forms a simple potential well.

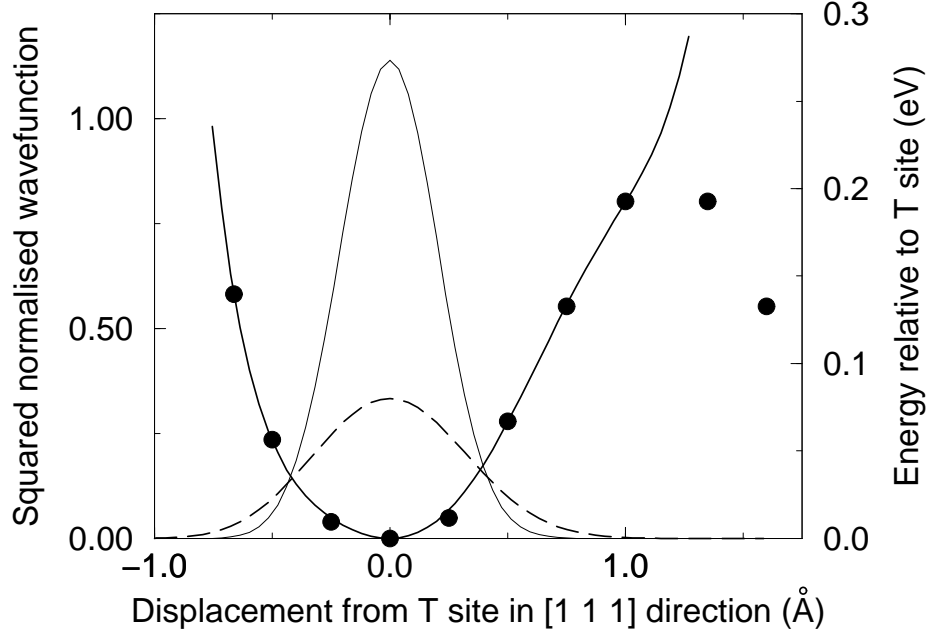


FIG. 6. The square of the proton (thin solid line) and muon (dashed line) wave functions at the T site in germanium. The symbols denote the potential well for the 16-atom supercell, and the thick solid line is the fit to Eq. 2.9 with the parameters of Table II. The potential has a maximum at the hexagonal site situated at 1.23 Å from the T site, but the fit has been constrained so that it forms a simple potential well.

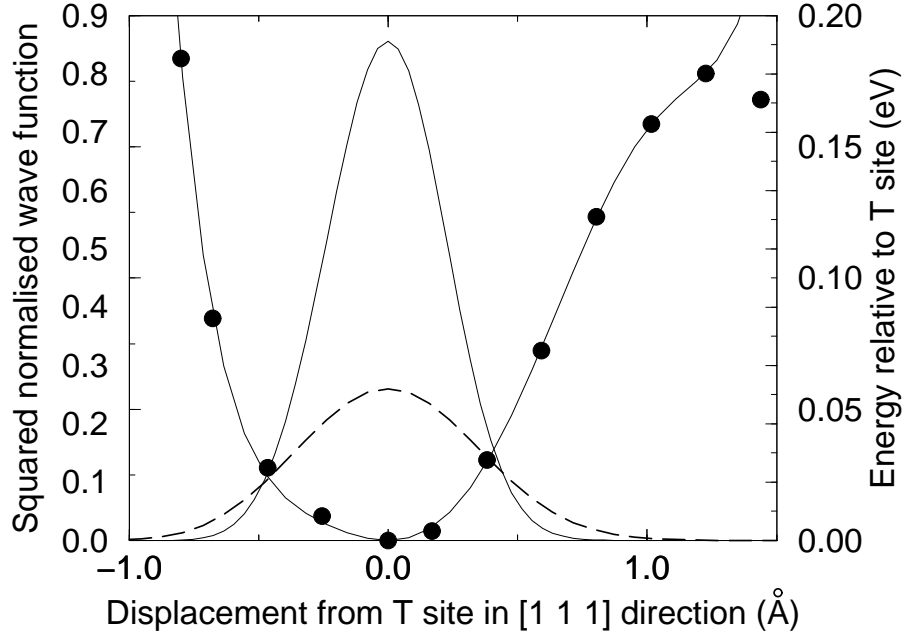


FIG. 7. Spin density contour map in the neighbourhood of (a) the BC site and (b) the T site in silicon. In (a) the muon position is located dead centre, with the two nearest-neighbour silicon atoms above and below. In (b) the large concentration of positive spin density is located on the muon position, the positions of nearby silicon atoms in this plane are indicated with crosses. Continuous, dashed and dot-dashed lines correspond to positive, negative, and zero values respectively. The separation between adjacent isodensity contours is  $0.001 \text{ e}/\text{bohr}^3$

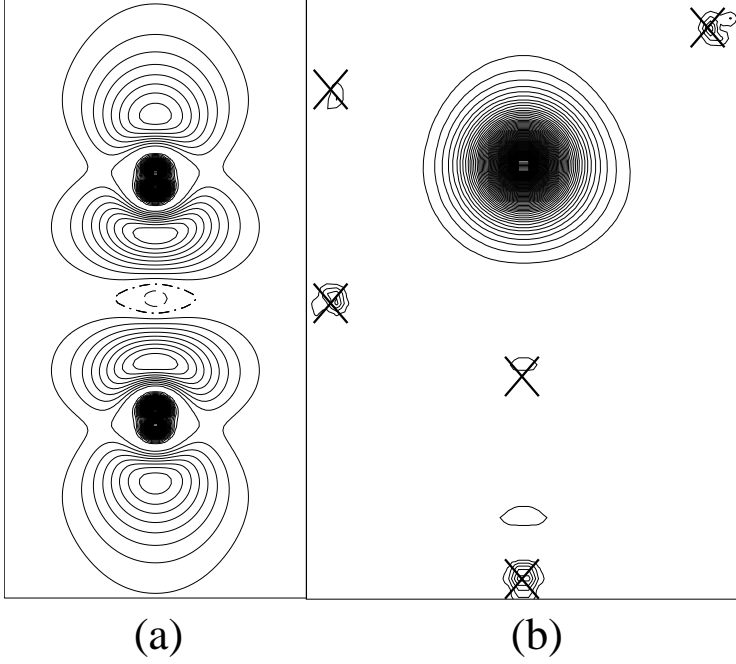


FIG. 8. Variation of the isotropic hyperfine parameter and the  $xy$  component of  $\mathbf{A}_p$  with displacement of the muon/proton from the BC site. The calculations were performed in silicon with the 16-atom supercell and the standard basis set. The lines are guides to the eye.

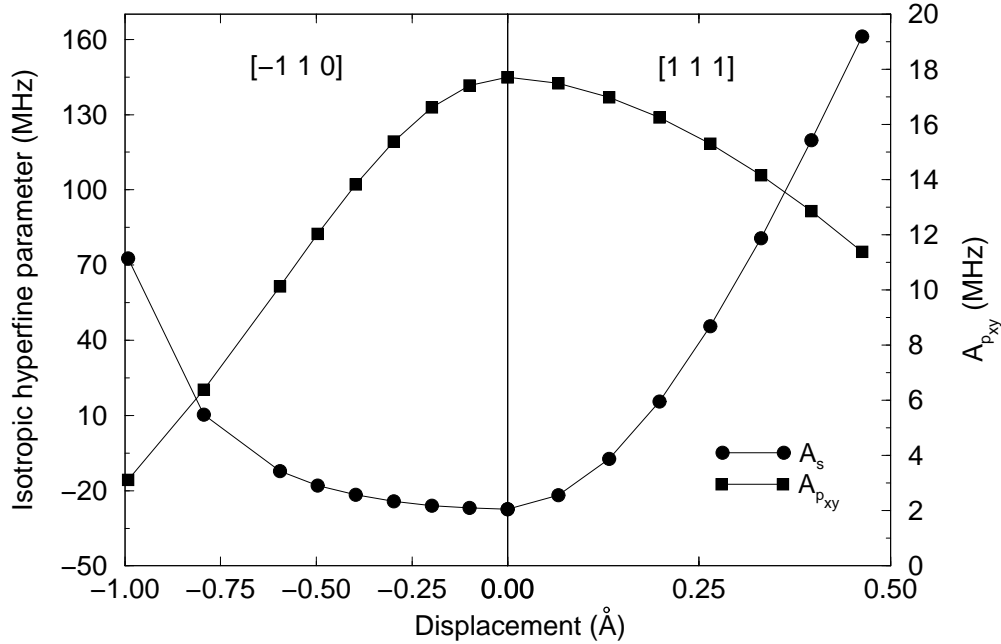


FIG. 9. The variation in the isotropic hyperfine parameter along the  $[1\ 1\ 1]$  direction at the T site in silicon (54-atom supercell) and germanium (16-atom supercell). A positive displacement indicates movement towards the hexagonal site. The lines are guides to the eye.

